Proceedings of the 15th International Heat Transfer Conference, IHTC-15
August 10-15, 2014, Kyoto, Japan

IHTC15-□□□□□

STUDY OF THE COMBINED EFFECTS OF LIQUID PROPERTIES AND SURFACE MICROPATTERNING ON POOL BOILING HEAT TRANSFER

E.Teodori[1], A. S. Moita[1*], A. L. N. Moreira[1]

[1]IN+ - Center for Innovation, Technology and Policy Research, Instituto Superior Técnico, University of Lisbon. Av. Rovisco Pais, 1049-001 Lisbon, Portugal

ABSTRACT

The present paper addresses the quantification of the various terms of the pool boiling heat transfer over micro-structured surfaces. The micro-structures are composed by regular patterns of quadrangular cavities, with fixed sizes, where only the distance between the center of the cavities, *S* is varied. The surfaces are made from silicon wafers. The wettability of the surfaces, quantified by the contact angles is not dramatically changed during the structuring process. The independent data required for bubble nucleation and heat transfer characterization are collected coupling high speed camera visualization, PIV (Particle Image Velocimetry) and heat flux/surface temperature measurements. The results confirm the relative importance of the induced bulk convection, particularly in the boiling of liquids with smaller values of the latent heat of evaporation (*e.g.* refrigerants). In this context, a more detailed characterization of the flow and of the bubble dynamics is presented. Based on this characterization, an alternative approach is suggested to correlate the experimental data with a modified Rohsenow formulation, using a characteristic bubbles' velocity to compute the Reynolds and the Stanton number, both associated to the bubble detachment and motion in bulk induced convection. Despite the devised relations still have an empirical nature, the work is in progress towards a more mechanistic and objective approach.

KEY WORDS: Boiling and evaporation, Heat transfer enhancement, Electronic equipment cooling, Micro-structured surfaces, Heat transfer correlations, Particle Image Velocimetry.

1. INTRODUCTION

During the last half of the twentieth century and particularly since the early thirties, numerous experimental and numerical investigations on pool boiling heat transfer have been reported in the literature, as extensively reviewed, for instance in [1]. Several strategies have been proposed to enhance pool boiling heat transfer, which mainly act on two distinct regimes: i) at low heat fluxes, in partial nucleate boiling, for which the heat transfer coefficient can be enhanced by promoting nucleation [2] and ii) at high heat fluxes, in the regime fully developed nucleate boiling, in which the main objective, besides having high heat transfer coefficients, *h* is to delay the occurrence of the critical heat flux CHF [3]. One of the most used strategies is altering the surface topography. However, by doing so, both topography and wettability are often simultaneously changed, in a non-systematic way. Following the classical wetting theories of Wenzel [4] and of Cassie and Baxter [5], which relate the surface topography with the wettability quantified as the contact angle, it is easy to understand that modifications of the surface topography easily lead to different wetting conditions, as the surface energy is altered during the roughening and/or coating processes. This issue has been recently raised by Bourdon *et al.* [6,7] who discuss the need to perform isolate experiments in which only chemical or topographical modifications are introduced on the surface. In addition, many authors use stochastically roughened surfaces, which disable any correlation between bubble formation and the surface topography, as

*Corresponding Author: anamoita@dem.ist.utl.pt

recently argued by McHale and Garimella [8]. Several authors on the other hand have chosen to work with regularly patterned surfaces (*e.g.* [9-10]), but universal agreement on the phenomena occurring at those surfaces (many of them related to interaction mechanisms) and on the optimal patterns to maximize pool boiling heat transfer have not been achieved yet. While surface wettability mainly plays a role on the onset of boiling and on keeping the nucleation stable (through contact angle hysteresis), so that it affects CHF [3], surface topography endorses the increase of active nucleation sites density, but also affects significantly the interaction mechanisms (*e.g.* [11,12]). In [11,12] one has explored the effect of surface topography on bubble dynamics and suggested a relation linking the distance between micro-cavities and the heat transfer coefficient. These studies produced interesting guiding results, but theoretical ground is still lacking to fully explain the observed trends. Particularly, modeling the heat transfer is not yet assessed. In this context, several authors prefer a mechanistic approach, focusing on the heat transfer occurring during bubble formation and detachment from the surface. For example, Corty and Foust [13] and Griffith and Wallis [14] argue that the micro-roughness of the boiling surface affects the position and slope of the nucleate boiling curve. Gaertner [15] reports that the nucleation site density fits the Poisson distribution, using the data of Gaertner and Westwater [16]. This was later confirmed by Sultan and Judd [17] and Del Valle and Kenning [18]. Also based on a mechanistic approach, Kandlikar [3] proposes a relation to predict the CHF, which explicitly includes the effect of the wettability quantified by the contact angle. Later, Chu *et al.* [19] and Gerardi *et al.* [20] revisited the correlation of Kandlikar to predict the CHF for pool boiling of water and nanofluids over micro-structured surfaces. Gerardi *et al.* [21], following the approach earlier suggested by Han and Griffith [22], also proposes that the heat removed during the boiling process is considered to be through the following contributions: the latent heat to form the bubble, the heat removed during the re-formation of the thermal boundary layer, or surface quenching heat flux and the heat transferred by turbulent natural convection outside the zone of interest of the bubbles.
Despite important breakthroughs in understanding and describing the fundamentals of pool boiling heat transfer have been achieved with these studies, the devised correlations are mainly semi-empirical, so they capture particular mechanisms that prevail under the specific working conditions for which the experimental data is obtained. Hence, despite it was proposed more than sixty years ago, general relations such as that of Rohsenow [23] are still studied and revisited, (*e.g.* Jabardo *et al.* [24]) and serve as basic formulation for recent theoretical approaches as that proposed by Betz [25].

In this context, the present paper addresses a mechanistic approach to evaluate the various mechanisms of pool boiling heat transfer, namely natural convection, evaporation associated to bubble formation and detachment and thermal boundary layer reformation that is endorsed by bubble detachment from the surface. Surface topography is systematically changed by regular patterns of quadrangular cavities, with fixed sizes, where only the distance between the center of the cavities, S is varied. The wettability of the surfaces, quantified by the contact angles is not dramatically changed. The independent data required for bubble nucleation and heat transfer characterization are collected coupling high speed camera visualization, PIV (Particle Image Velocimetry) and heat flux/surface temperature measurements. After this evaluation, an alternative approach is suggested to correlate the experimental data with a modified Rohsenow formulation, using a weighted characteristic bubbles' velocity to compute the Reynolds and the Stanton number, both associated to the bubble detachment and motion in bulk induced convection. This relation is a work in progress and therefore is still subjected to the empirical nature related to the particular working conditions and geometry of the present experimental work.

2. EXPERIMENTAL ARRANGEMENT AND DIAGNOSTIC TECHNIQUES

Pool boiling is investigated for various liquids, namely the dielectric fluid HFE 7000, ethanol and water. These fluids were selected since they can cover a wide range of the values of surface tension and of the relevant thermal properties such as the thermal conductivity, the heat capacity and the latent heat of evaporation, as shown in Table 1.
Heat flux and heat transfer coefficients are determined for all liquid/surface combinations used in the present work. Afterwards, they are related to the bubble dynamics. This characterization is made by combining high-speed visualization with PIV measurements.

The structured surfaces are custom made from silicon wafers. These wafers are coated with aluminum (to allow a deeper etching) and afterwards with photoresist. The regular patterns are transferred by high resolution printing (performed at INESC-MN) and photolithography and are then submitted to plasma etching for 5-7hours. This procedure assures the anisotropic etching to create the required dimensions of the micro-patterns. Finally, wet etching is used to remove the aluminum coating. The surfaces are micro-structured with regular arrays of squared cavities, with fixed size length a=52 µm and fixed depth h_R=20µm. The distance between the centers of the cavities, S is mainly the only variable distance, ranging between 300µm<S<1200µm. The parameters characterizing the micro-patterns are schematically defined in Fig. 1, together with a photo of one of the surfaces. Slight rounding of the edges of the square cavities may occur, but the apparent round shape of the cavities in Fig. 1 is an optical distortion caused by the positioning of the camera. The surfaces were characterized by their surface topography (from roughness profile meters) and by the wettability quantified by the contact angle. Roughness profiles were measured using a Dektak 3 profile meter (Veeco) with a vertical resolution of 200Angstroms. Wettability was also characterized, being quantified by the static contact angle θ, using an optical tensiometer THETA from Attesion, with One-Attesion v1.8 software. Accuracy of the measures of the contact angle is ±1º, according to the manufacturer. Table 2 depicts the main topographical characteristics of the surfaces used in this study. The table includes the average values of the static contact angles, which were measured as described in [26]. The contact angles obtained with ethanol and HFE7000 in contact with all the surfaces are close to zero.

Table 1 Thermophysical properties of the liquids used in the present study, taken at saturation, at 1.013x10^{5}Pa.

Property	Water	Ethanol	HFE7000
T_{sat} (°C)	100	78.4	34
ρ_l (kg/m^3)	957.8	736.4	1374.7
ρ_v (kg/m^3)	0.5956	1.647	4.01
μ_l (mN m/s^2)	0.279	0.448	0.3437
c_{pl} (J/kgK)	4217	3185	1352.5
k_l (W/mK)	0.68	0.165	0.07
h_{fg} (kJ/kg)	2257	849.9	142
σ_{lv} (N/m)x10^3	58	17	12.4

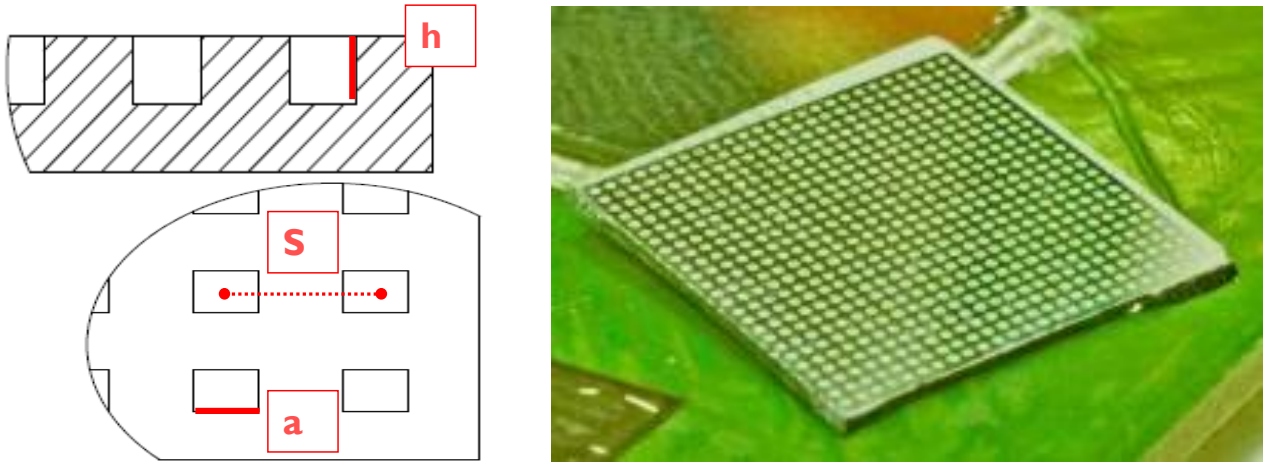

a) **b)**

Fig. 1 a) Identification of the main parameters quantifying the micro-patterns. **b)** Sample of one of the micro-structured surfaces.

The experimental arrangement is composed by a power supply, the pool boiling test section (Fig 2a), a high-speed camera (Phantom v4.2 from Vision Research Inc., with 512x512pixels@2100fps and a maximum

frame rate of 90kfps), a DAQ acquisition system (Fig 2a) and a PIV system. The temperatures are sampled using type K thermocouples. The signal is acquired and amplified with a National Instruments DAQ board plus a BNC2120. The acquisition frequency is 100Hz and the temperature is monitored for 20 seconds after reaching a stable condition (constant temperature variation which does not exceed ±0.5°C). The entire heating section of the pool boiling test section is isolated with Teflon. The liquid is pre-heated and degassed in a pre-chamber. The refilling and the entire measurement processes are automatically controlled using a number of valves. The system responds based on the information provided by a pressure transducer (OMEGA DYNE Inc). The control system reacts to pressure variations in the order of 5mbar. Heaters disposed on the sides of the pool boiling chamber are controlled by a PID controller to assure that the liquid remains inside the chamber at saturation temperature. Detailed description of the experimental set-up is provided in [11,12].

Table 2 Main range of the topographical characteristics of the micro-patterned surfaces. θ is the average static contact angle measured with water at room temperature. θ≅0º for all the surfaces in contact with ethanol and HFE7000.

Material	Reference	a [µm]	h_R [µm]	S [µm]	θ [º]
Silicon Wafer	Smooth	≈ 0	≈ 0	≈ 0	86.0
	C1	52	20	304	90.0
	C2	52	20	400	91.5
	C3	52	20	464	71.5
	C4	52	20	626	86.5
	C5	52	20	700	95.0
	C6	52	20	800	60.5
	C7	52	20	1200	66.3

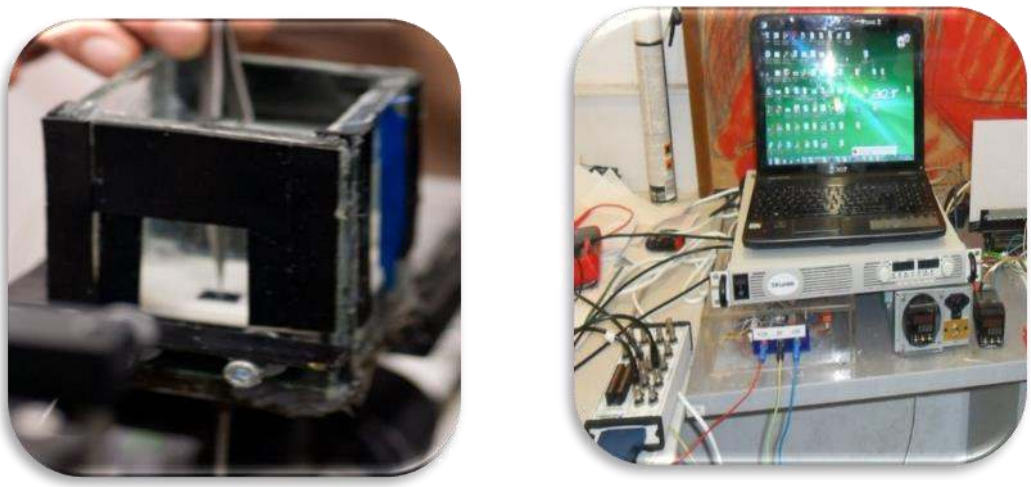

a) **b)**

Fig. 2 a) Detail of the pool boiling section, **b)** DAQ system.

2.1 Heat Transfer Measurements

The boiling curves are presented for each liquid and each heating surface by varying the imposed heat flux in steps of 1-5W/cm^2. Each curve is obtained from the average of four experiments, as illustrated in Fig.3. It is worth mentioning that the entire curve is not represented here, but only the part which is relevant for our results.

The main uncertainties of the quantities related to the heat transfer measurements are summarized in Table 3. The uncertainty in the temperature measurements is assessed according to [27]. The maximum combined uncertainty is the maximum value of uncertainty obtained for all the pairs liquid/surface tested.

Table 3 Main uncertainties of the quantities related to the heat transfer measurements.

Measured parameter	Maximum combined uncertainty	Evaluation method
Heat flux q" [W/cm^2]	±22.5% (fully developed nucleate boiling of HFE7000)	$\frac{\Delta q''}{q''} = \left[\left(\frac{\Delta L}{L}\right)^2 + \left(\frac{\Delta T}{T}\right)^2\right]^{1/2}$ L is the thickness of the heating surface for which the heat flux is evaluated
Temperature T [ºC]	±22.5%	$unc_T = \left[B^2 + t_{95}\sigma^2\right]^{1/2}$ B is the bias limit, t_{95} is the confidence level and σ is the standard deviation
Heat transfer coefficient h [W/cm^{2}K]	±22.5% (fully developed nucleate boiling of HFE7000)	$\frac{\Delta h}{h} = \left[\left(\frac{\Delta q''}{q''}\right)^2 + \left(\frac{\Delta T}{T}\right)^2\right]^{1/2}$

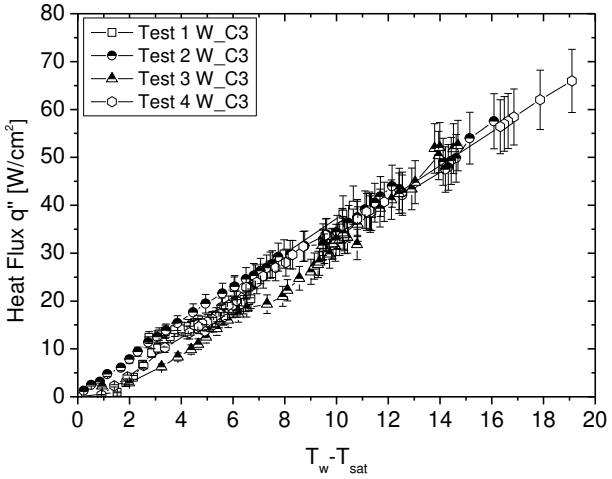

Fig.3 Example of the 4 boiling curves taken in each experiment. In this case these curves correspond for pool boiling of water over surface C3 (S=464μm).

2.2 Image Post-Processing for the Characterization of Bubble Dynamics

Following an approach similar to that presented in many works reported in the literature, the parameters selected here to characterize bubble nucleation are the bubble departure diameter, the bubble departure frequency and the active nucleation sites density. This characterization is based on high-speed visualization and image post-processing. The images are recorded with a frame rate of 2200fps. For the optical configuration used here, the spatial resolution is 9.346μm/pixel.

The bubble departure diameter is measured for each test condition from 300 to 1060 frames. For each image a mean value is averaged from 5-16 measurements for every nucleation site that is identified in the frame.

The accuracy of the measurements of the bubble departure diameter is ±9.346 μm. Coalescence effects are confirmed based on visual inspection of the processed images.

The bubble departure frequency is estimated by determining the time elapsed between apparent departure events, which are counted for a defined interval of time. The departure frequency is assessed, for each test condition, for at least five nucleation sites, which are evaluated based on extensive image post-processing of 300 to 1060 frames. The final value of the bubble departure frequency is the average between the frequencies of each nucleation site. The uncertainty associated to these measurements is ±1 fps.

Finally, the evaluation of the active nucleation sites density must be done by visual inspection of the frames, which introduces an uncertainty associated to the subjective criterion of the observer. To lessen this uncertainty, at least ten frames are chosen, at different times during the single experiment. The nucleation sites are identified on each frame. The final values of the active nucleation site density are an average of the ten evaluated values for the same region of interest. Fig. 4 illustrates some images used in the post-processing procedures. Table 4 summarizes the uncertainties of the main quantities related to the bubble parameters.

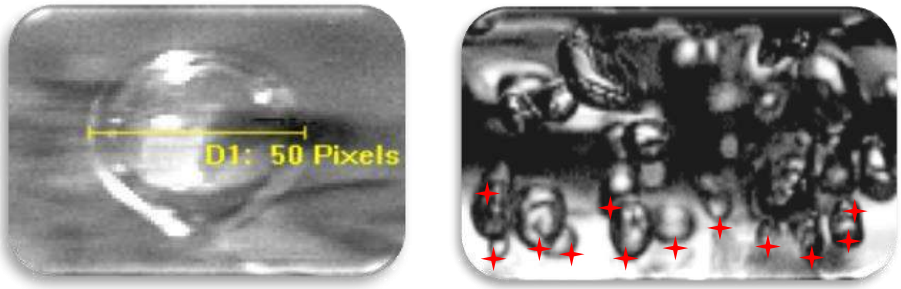

a) **b)**

Fig.3 Illustrative images used for the post-processing procedures. **a)** Evaluation of the bubble departure diameter, **b)** Detection of the nucleation sites.

Table 4 Main uncertainties of the quantities related to the measurements of the bubble parameters.

Measured parameter	Maximum combined uncertainty	Evaluation method
Bubble departure diameter D_b [mm]	±9.3% (HFE7000)	$\frac{\Delta D_b}{D_b} = \frac{\pm 2\,px.(mm/\,px)}{D_b}$
Bubble departure frequency [Hz]	±19.7% (Ethanol)	$\frac{\Delta f_b}{f_b} = \frac{\{n_{events}/(n_{frasmes}+2).fps\}}{f_b}$
Nucleation sites density NSD [m^{-2}]	±34.8 % (Ethanol)	$\frac{\Delta NSD}{NSD} = \frac{(NSD \pm \sigma)}{NSD}$

2.3 Particle Image Velocimetry (PIV) Measurements

Following the procedure suggested by [29] seeding is not used, but instead the bubbles are tracked. Bubbles' diameter is in the range of 500-800 µm, measured by image post-processing. These dimensions and the low characteristic velocities of the bubbles (1-10 cm/s) require a careful analysis of all the parameters which have to be selected in the PIV configuration. The PIV system uses a CCD camera Kodak Megaplus, Model 1.0, with an image resolution of 1018x1008 $pixel^2$. The bubbles are illuminated via a dual Nd:YAG Litron laser. The time delay between laser pulses is varied ($1<\Delta t<8$ms) depending on the imposed heat flux: the time between pulses is smaller for higher imposed heat fluxes. Furthermore, the interrogation area and the overlap are also varied for the various imposed heat flux conditions, in an optimization process, to assure that the chosen values are adequate to obtain accurate measurements. Hence, the selected interrogation area was varied between 16 and 64 pixels (1pixel/58µm) to assure that at least five bubbles are inside. An overlap of 50% is chosen by analyzing two consecutive frames and evaluating the average displacement of the bubbles. The most appropriate approach for this kind of flow is using a recursive cross correlation or the average correlation algorithms (*e.g.* [28]). In the present work, after analyzing extensively both approaches, the cross correlation was considered to be the most appropriate. The measurements performed using PIV are

compared with extensive image post-processing, within quite good agreement. The PIV data were processed with the software Flow manager 4.2. Detailed description of this procedure is given in [12].

3. RESULTS AND DISCUSSION

A detailed analysis of bubble dynamics, namely bubble departure frequency and diameter, as well as nucleation sites density was earlier presented in Teodori *et al.* [29]. Based on a force balance performed to the bubble at detachment, those results clearly show that the largest bubbles are formed during the boiling of the fluid with the largest surface tension (water). The departure frequency is similar for most of the surfaces, for the three liquids, but there is a significant reduction of the frequency of the water bubbles, for the surface with the smallest *S*, which is associated to an excessively promoted coalescence. Hence, it was concluded that for liquids with larger surface tension (water), the coalescence factor $D_b/D >> 1$ (being D_b the averaged bubble diameter and D the diameter as the bubble exits the cavity, i.e. with no coalescence) is quite large and varies significantly with *S*, thus evidencing the strong coalescence effects observed at water boiling. Such strong coalescence effect lessens the bubble departure frequency and creates several blockages to a regular bubble departure, as the large bubbles obstruct the nucleation sites, insulate the surface and preclude the liquid motion. Given the highest latent heat of evaporation that is required to vaporize water, all the boiling process is actually lessened. As the cavities are too close, the interaction phenomena become dominant and lead to the steep deterioration of the heat transfer coefficient (which occurs for instance for surface C1 (S=304 μm). On the other hand, for well wetting fluids (ethanol and HFE7000), with low surface tension, the coalescence factor is not much larger than 1, so interaction mechanisms are less evident. In line with this, the boiling curves and the heat transfer coefficients determined in Teodori *et al.* [29] show that ethanol and HFE 7000 present a more homogenous and vigorous boiling, with limited interaction mechanisms, so there is a monotonic raise of the heat transfer coefficient for the micro-patterned surfaces, as the distance between cavities *S* decreases, i.e. the number of nucleation cavities increases. Given that the bubble interaction mechanisms are lessened for these fluids, numerous smaller bubbles regularly detach from the surface without blockage of large vapor bubbles. The overall departure frequency also increases for surfaces with more cavities (smaller S), so the increase of the number of cavities leads to an effective increase of the active nucleation sites density, thus improving the pool boiling heat transfer. In line with this, the coalescence effects can be empirically related to the distance *S*, given that this is directly acting on the coalescence mechanisms which occur close to the surface. Considering the characteristic bubble size obtained by the force balance describing the bubble detachment, as proposed by Fritz [30] and followed by many other researchers: $L_c=(\sigma_{lv}/(g.(\rho_l-\rho_v))^{1/2}$ a dimensionless distance can be obtained S/L_c which empirically translates the evolution of the heat transfer coefficient following the trends described above. This empirical relation, earlier suggested in [11] is extended for ethanol and HFE7100 pool boiling as presented in Fig. 5.

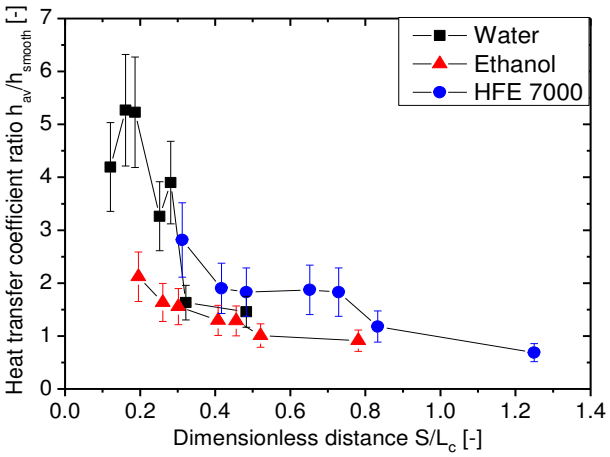

Fig. 5 Heat transfer ratio vs dimensionless distance for water, ethanol and HFE 7000 in the range of patterns studied.

This representation already allows accounting for the relative improvement of the performances using the micro-patterned surfaces since, it compares the enhancement of the heat transfer coefficient using each micro-structured surface (each surface with different *S* corresponds to each of the single points in the plot) with that of the smooth surface. It is worth mentioning that h_{av} are mean values obtained for the region of fully developed boiling, for which all the measured values (for each surface) clearly tend to collapse around a mean value. This trend is taken for all the liquid/surface pairs used to produce the data points in Fig.5.
The distance *S* is in turn related to the characteristic bubble departure dimensions. This relation is important as it defines the critical distance *S* up to which the bubbles with a certain diameter, depending on the balance between surface tension and buoyancy forces ($L_c=(\sigma_{lv}/(g.(\rho_l-\rho_v))^{1/2}$) will coalesce. So, for well wetting fluids, for which the coalescence factor is not too high and the interaction mechanisms are not dominant, an effective increase of the number of cavities corresponds to lower values of S/L_c. As discussed above, lower values of *S* and therefore lower values of S/L_c give rise to a better bubble dynamics and overall pool boiling heat transfer performance, which are translated in Fig.5 by higher values of h_{av}/h_{smooth}. For low wetting fluids such as water, decreasing S/L_c is advantageous until a maximum value of *S*, for which the coalescence factor is too high (surface C1 S=304 μm). For such values of *S* the negative effects of bubble interaction become dominant and lead to a deterioration of the heat transfer coefficient, so that h_{av}/h_{smooth} decreases. This is the effect observed for the lowest values of S, which correspond to the lowest values of S/L_c in Fig. 5.

However, the values of the heat transfer coefficients represented in Fig. 5 include, as aforementioned, the various contributions to the heat flux. To infer on the relative importance of each of these, a mechanistic approach was followed. Following previous authors (*e.g.* [20-22,31]), three main boiling mechanisms are evaluated: natural convection $q''_{nat\ conv}$, evaporation q''_{ev} and induced convection or quenching q''_{q}, which are respectively given by:

$$q''_{natconv} = \left[1 - \frac{\pi}{4A}\sum_{n=1}^{N_T}\left(D_{b,n}\right)^2\right] h_{natconv}\left(T_w - T_{sat}\right) \tag{1}$$

$$q''_{ev} = \frac{\pi}{6A}\rho_v h_{fg}\sum_{n=1}^{N_T}\left(f_{bn}.D_{bn}^3\right) \tag{2}$$

$$q''_{q} = \frac{2\pi k_l (T_w - T_{sat})}{A\sqrt{\pi\alpha_l}}\sum_{n=1}^{N_T}\left(D_{bn}^2.\sqrt{t_{wn}}\, f_{bn}\right) \tag{3}$$

Here, *A* is the area of the heater, N_T is the total number of nucleation sites, N_{ac} is the number of active nucleation sites, t_{wn} is the waiting time and $\alpha_l=k_l/\rho_l C_{pl}$ is the liquid thermal diffusivity. $h_{natconv}$ was estimated considering the correlation of McAdams [31], for natural convection over a horizontal plate. The errors associated to the various quantities that were determined experimentally were taken into account by error propagation, considering the inaccuracies summarized in Table 4. Nevertheless although qualitatively correct, quantitatively this is only an estimative which must still include additional parameters.
The relative importance of the contribution to the total heat flux associated to bubble evaporation q''_{ev} and to the induced bulk convection q''_{q} is represented in Fig. 6. The figure shows that the heat removed due to bubble evaporation can be of the same order or even lower than that of the induced bulk convection, particularly for the well wetting liquids boiling over the surfaces with more cavities (smaller values of *S*). This is related to the overall enhanced bubble dynamics and better boiling performance of such liquids over those surfaces with smaller *S*, as discussed in the previous paragraphs. Indeed, the evaporation contribution associated to the boiling of water is only larger for the surfaces with higher *S*, for which the boiling performance mainly depends on the thermal properties of the liquids. The mechanism of the bulk induced convection is naturally dependent on the bubble parameters which become very high for the boiling of such low wetting liquids over enhanced surfaces (*e.g.* bubble departure frequency), but looking at the fluid dynamics it is also associated to the bubble detachment and to the induced bubble flow, which in turn should be related to the bubble vertical velocity. This is a logical step considering that most of the existing

correlations (including that of Rohsenow) are a function of Reynolds and Prandtl numbers. To infer on this possible relation, bubbles' vertical velocity was evaluated by PIV measurements, following the procedure introduced in Teodori *et al.* [12]. The average vertical bubble velocity (average of the velocity profile for a fixed value of H/D) was evaluated along the vertical dimensionless distance *H/D*, where *H* is the vertical distance from the top face of the surface in (mm) and *D* is the bubble departure diameter (also in mm), for different heating conditions and different micro-patterns. The velocity profiles are presented for the surfaces with the smallest and the largest distance between cavities in Fig. 7.

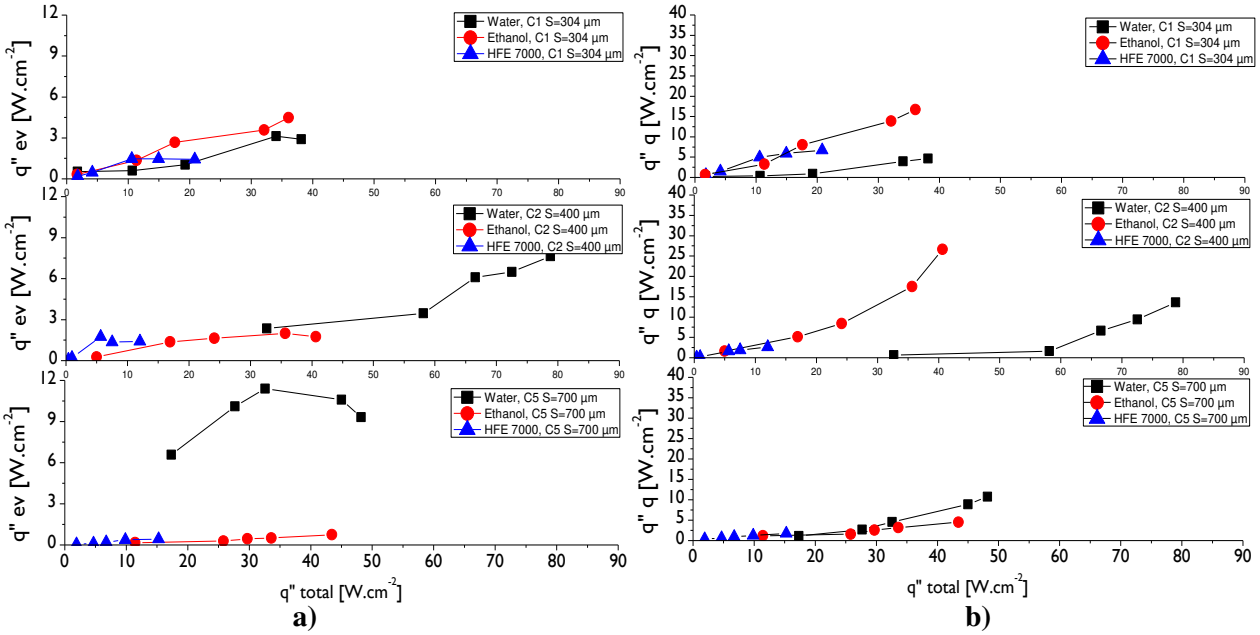

Fig. 6 Evaluation of the relative importance of **a)** the evaporation term and **b)** the induced bulk convection term in comparison to the total heat flux.

It is worth noting that the vertical velocity profiles are only presented here for ethanol, due to paper length restrictions, although similar trend is observed for HFE7000. Overall, the plots show that bubbles are ejected with larger average velocity, as the imposed heat flux is higher. Then they decelerate due to the braking effect forced by the zero velocity at the top of the pool. Surfaces with closer cavities (C2 S=400µm) present more uniform and stable profile when compared to those with sparser cavities (C7 S=1200µm), for which the velocity profiles can be very disturbed, particularly at higher heat fluxes. Hence, the cavities, for these fluids, seem to act as stabilization factor to the vertical velocities. This is in agreement with our previous findings (Teodori *et al.* [11]).

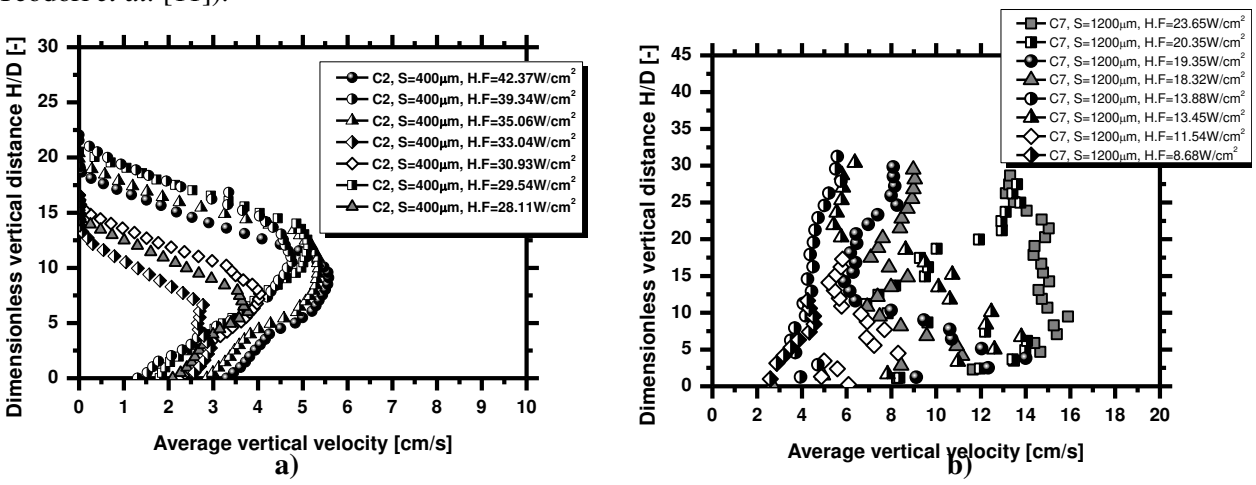

Fig. 7 Vertical velocity profile for HFE 7000 boiling over micro-patterned surfaces: **a)** C2 S= 400µm and **b)** C7 S= 1200µm.

Fig 8 depicts the global heat transfer coefficients (as used to compute Fig. 5) as a function of the average bubbles' vertical velocities for ethanol and HFE700 boiling over the micro-structured surfaces with smallest and largest *S*. It is now evident that the bubbles' vertical velocity is larger for HFE7000 than for ethanol, particularly for the boiling over the surfaces with smaller *S*. Also, the heat transfer coefficient follows a more stable increase with the bubble's characteristic velocity for this surface, when compared to that of ethanol. Considering the importance of the induced bulk convection in these fluids, the highest heat transfer coefficient that was obtained for the boiling over the surface with smaller *S* cannot be solely attributed to the increase of nucleation sites, but may also be related to the flow and to the stabilization effect of the micro-patterns. The heat transfer coefficient for ethanol pool boiling is less sensitive than that obtained for HFE7000 to the characteristic bubble velocity, as this fluid still has quite a high value of the latent heat of evaporation and the term of bubble evaporation is definitely quite relevant. This argument however, must still be confirmed with further and more detailed investigation on the bubble detachment velocity, closer to the surface. Nevertheless, based on the whole analysis performed so far, one can argue that the term of induced bulk convection is quite important for booth ethanol and HFE7000. Consistently, the heat transfer coefficient seems to be related to the characteristic bubbles' velocity.

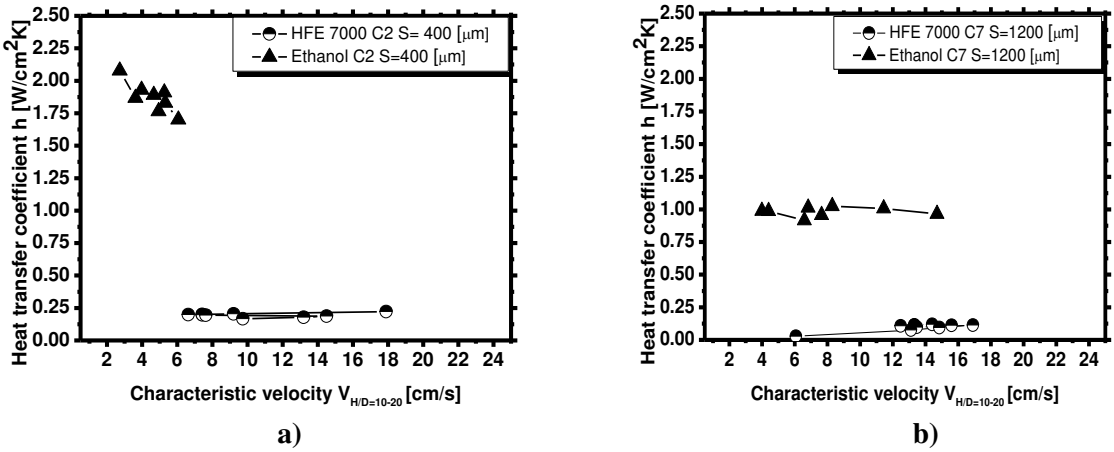

Fig. 8 Heat transfer coefficient as a function of the characteristic velocity $V_{H/D}$ for ethanol and HFE 7000 boiling over: **a)** Surface C2 (S=400μm) and **b)** Surface C7 (S=1200μm).

To infer how well this correlation could be established, some preliminary parametric studies were performed. Revisiting the formulation of Rohsenow [23] which also favors the effect of the induced bulk convection, one can write it in the reduced form:

$$St^* = C_{sf}\ Re_b^m\ .Pr_l^n \tag{4}$$

Here, St^* is the inverse of the Stanton number $St=h/(\rho V_{carat.}.c_p)$, P_{rl} is the liquid Pradtl number and Re_b is the Reynolds number associated to bubbles' departure diameter. *m* and C_{sf} are fitting parameters being the later classically related to surface properties. However instead of using the superficial velocity of the liquid and $(\sigma_{lv}/(g.(\rho_l-\rho_v))^{1/2}$ as the characteristic length scale, one used the experimental values of D_b (which were related to the heat flux in Teodori *et al.* [26]) and the characteristic bubbles velocity. This velocity, weighted by the ratios of the vapor and the liquid densities, to account for the buoyancy effect, was also used to compute a modified Stanton number *St'*.

As a preliminary exercise, C_{sf} was empirically related to the surface geometry, represented by S/Lc using a correlation of the type:

$$C_{sf}=aln(S/L_c)+b \tag{5}$$

as suggested in [24] (Fig.9). Qualitatively the results depicted in Fig. 9 agree well with those of [24] which show that the C_{sf} tends to increase for more smooth surfaces.

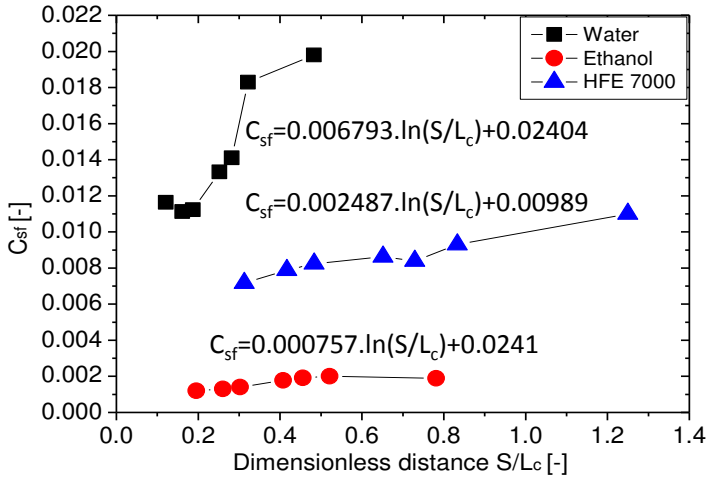

Fig.9 Empirical correlation of C_{sf} with the dimensionless distance S/L_c.

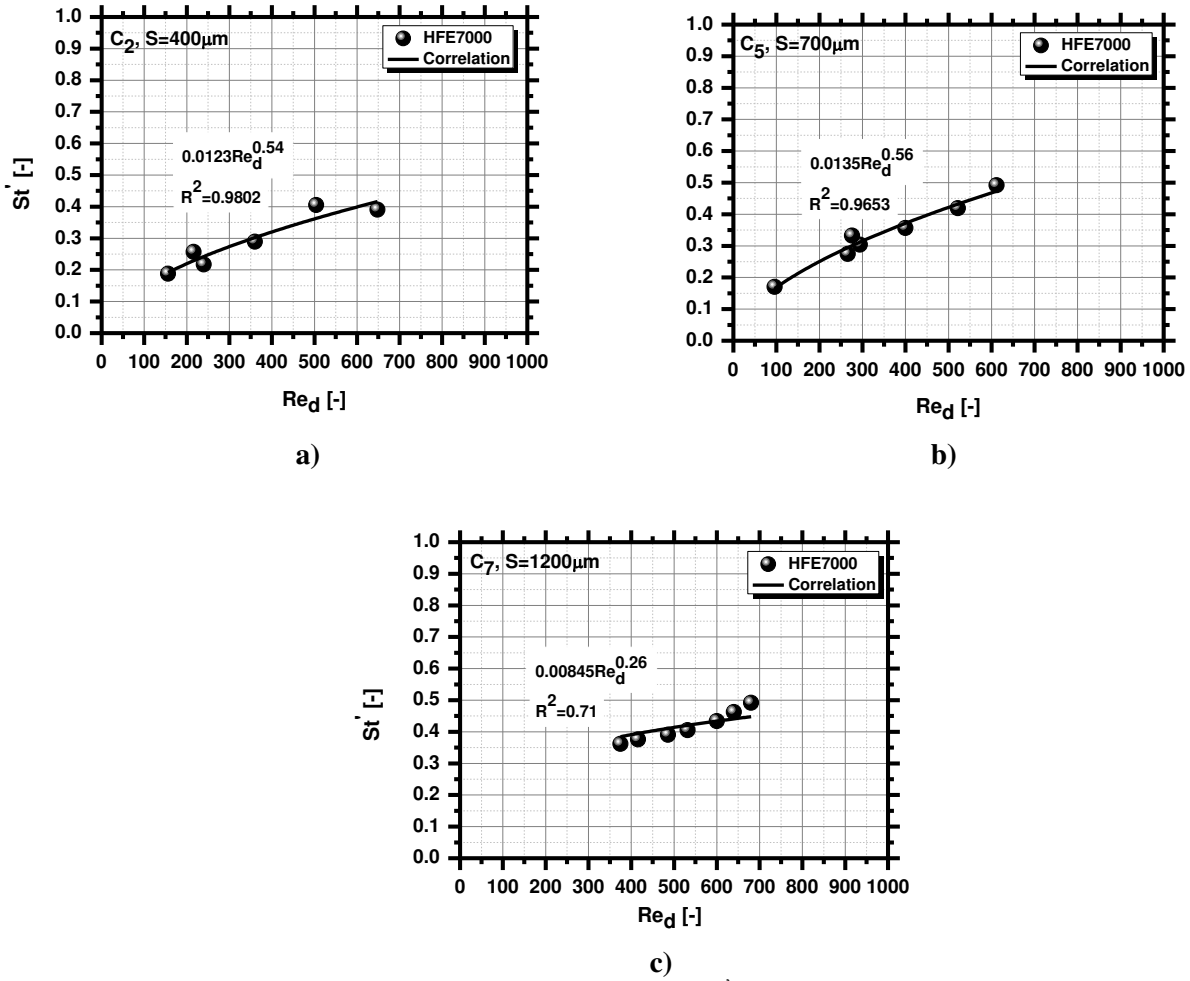

Fig.10 Correlation between the modified Stanton number St' and the Reynolds number based on bubble detachment diameter and scaled with bubbles' characteristic velocity for HFE7000 boiling over: **a)** C2, S=400µm, **b)** C5, S=700µm and **c)** C7, S=1200µm.

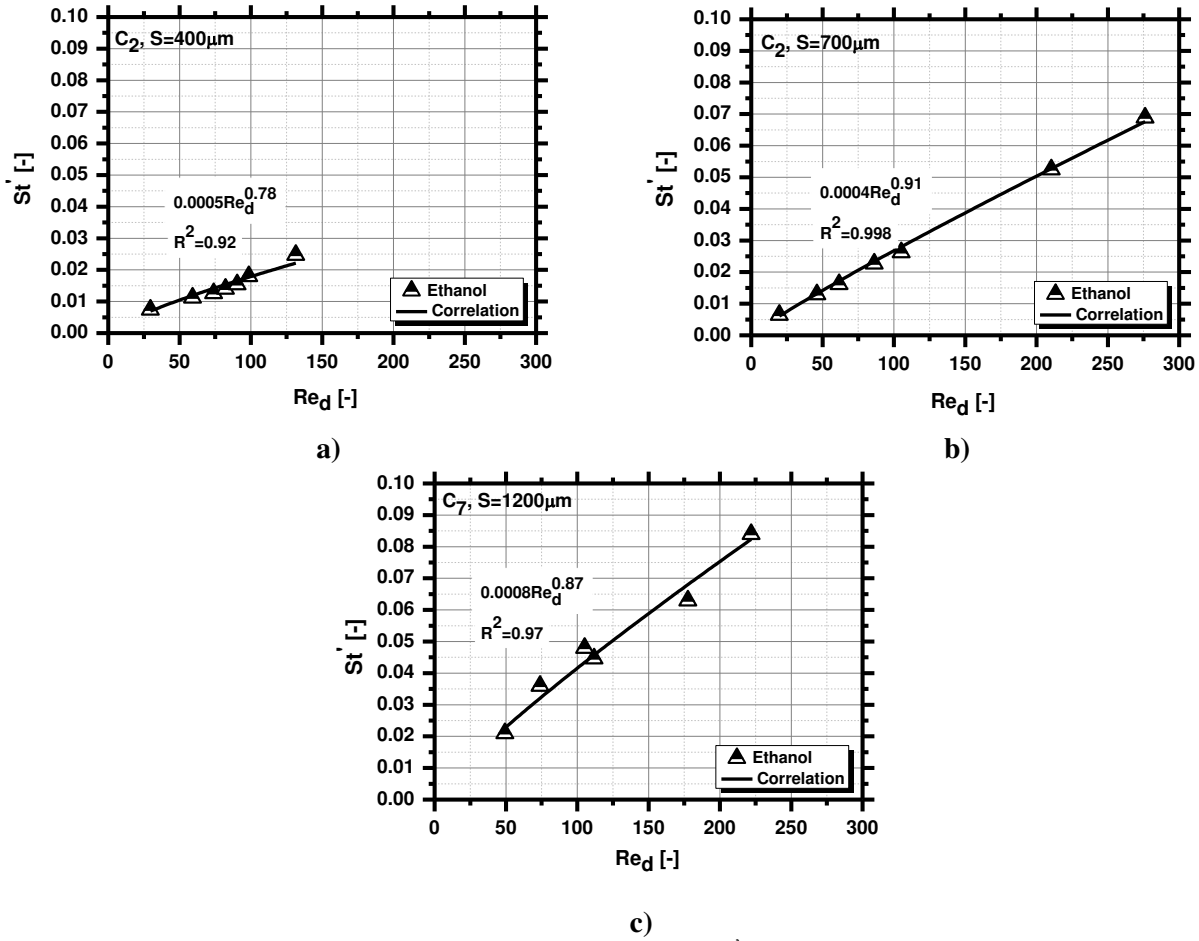

Fig. 11 Correlation between the modified Stanton number St' and the Reynolds number based on bubble detachment diameter and scaled with bubbles' characteristic velocity for ethanol boiling over: **a)** C2, *S*=400μm, **b)** C5, *S*=700μm and **c)** C7, *S*=1200μm.

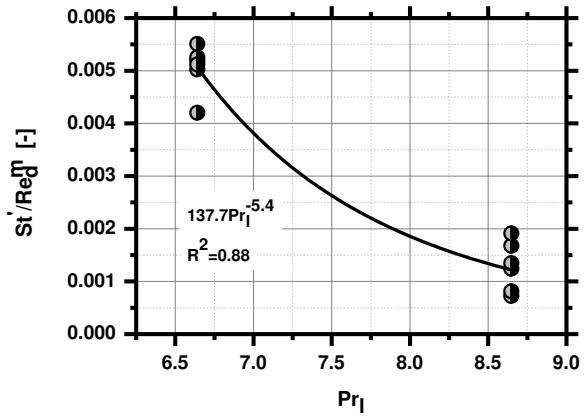

Fig. 12 Correlation between the experimental data and our empirical modified Rohsenow equation.

The results are presented separately for ethanol and HFE7000 boiling over different micro-structured surfaces, to detect dependencies of the fitting parameters with the liquid and with the surface properties. These results show that the scaling suggested in this paper can be used to correlate both ethanol and HFE700 data. This scaling, including the characteristic bubbles' velocity already captures part of the effect of the surface structuring (in the velocity). However, it still does not capture the interaction effects, which should be further investigated together with the coalescence factor. In that case, surface the fitting parameter C_{sf} is a

non-trivial function of *S*, and consequently of the number of cavities, N_c, the number of active nucleation cavities, N_{ac} and of the departure frequency, which are all correlated to *S* and will in turn affect the heat transfer coefficient, *h*. This is work in progress, which involves a detail that is out of the scope of the current paper.

6. CONCLUSIONS

The work presented here addresses the quantification of the various terms of the pool boiling heat transfer over micro-structured surfaces, following a mechanistic approach. The micro-structures are composed by regular patterns of quadrangular cavities, with fixed sizes, where only the distance between the center of the cavities, *S* is varied. The data required for bubble nucleation and heat transfer characterization are collected coupling high speed camera visualization, PIV (Particle Image Velocimetry) and heat flux/surface temperature measurements. The results confirm the important role of the induced bulk convection, particularly in the boiling of liquids with smaller values of the latent heat of evaporation. In this context, a more detailed characterization of the flow and of the bubble dynamics is presented. Afterwards, an alternative approach is suggested to correlate the experimental data with a modified Rohsenow formulation, using a characteristic bubbles' velocity to compute the Reynolds and the Stanton number, both associated to the bubble detachment and motion in bulk induced convection.

ACKNOWLEDGMENT

The authors are grateful to Fundação para a Ciência e a Tecnologia (FCT) for partially financing the research under the framework of project PTDC/EME-MFE/109933/2009 and to support E. Teodori with a PhD Fellowship (Ref.:SFRH/BD/88102/2012). A.S. Moita also acknowledges the contribution of FCT for Post-Doc Fellowship (Ref.:SFRH/BPD/63788/2009).

NOMENCLATURE

a	side length of the square cavities	(μm)
A	area of the heated	(m^2)
$c_{p,l}$	liquid specific heat	(J/kgK)
C_{sf}	fitting coefficient associated to surface properties	(-)
D_b	bubble departure diameter	(mm)
f_b	bubble departure frequency	(s^{-1})
g	constant of gravity acceleration	(m^2/s^2)
h	heat transfer coefficient	(W/cm^2K)
H	vertical distance from the surface	(mm)
h_{fg}	latent heat of evaporation	(kJ/kg)
h_R	depth of the square cavities	(μm)
k_l	liquid thermal conductivity	(W/mK)
L	thickness of the heated wall	(m)
m	fitting parameter	(-)
n	fitting parameter	(-)
N_{ac}	number of active cavities	(-)
N_c	number of cavities	(-)
N_T	total number of cavities	(-)
Nu	Nusselt number	(-)
Pr_l	Prandtl number of the liquid	(-)
q''	heat flux	(W/cm^2)
Re_d	Reynolds number associated to the bubble departure diameter	(-)
S	distance between the centers of the cavities	(μm)
St	Stanton number	(-)
St^*	Inverse of the Stanton number	(-)
St'	modified Stanton number using a weighted value of bubbles' vertical velocity	(-)
T	temperature	(ºC)
T_{sat}	saturation temperature	(ºC)
T_w	surface temperature	(ºC)
t	time	(s)
$V_{H/D}$	characteristic bubble vertical velocity	
Δt	time interval	(s)
α	thermal diffusivity	(m^2/s)
μ_l	liquid dynamic viscosity	(mN m/s^2)
θ	equilibrium contact angle	(º)
ρ_l	liquid density	(kg/m^3)
ρ_v	vapour density	(kg/m^3)
σ_{lv}	liquid surface tension	(N/m)
σ	standard deviation	

REFERENCES

[1] Manglik, R.M., Bergles, A.E., "Enhanced Heat and Mass Transfer in the New Millennium: A Review of the 2001 Literature", *J. Enhanced Heat Transf.*, 11, pp.87-118, (2004).

[2] Lee, D., Omolade, D., Cohen, R.E., Rubner, M.F., "pH-Dependent Structure and Properties of TiO2/SiO2 Nanoparticle Multilayer Thin Films", *Chem. Mater*., 19, pp.1427–1433, (2007).

[3] Kandlikar, S.G., "A Theoretical Model to Predict Pool Boiling FC Incorporating Effects of Contact Angle and Orientation", *J. Heat Transfer*, 123, pp.1071–1079 (2001).

[4] Wenzel, R.N., "Resistance of Solid Surfaces to Wetting by Water", *Industrial and Eng. Chem.*, 28, pp.988-994, (1936).

[5] Cassie, A.B., Baxter, S., "Wettability of Porous Surfaces", *Trans. Faraday Society*, 40, pp.546-551, (1944).

[6] Bourdon, B., Rioboo, R., Marengo, M., Gosselin, E., De Comninck, J., Influence of the Wettability on the Boiling Onset", *Langmuir*, 8, pp.1618-1624, (2012).

[7] Bourdon, B., B., Di Marco, P., Rioboo, R., Marengo, M., De Coninck, J., "Enhancing the Onset of Pool Boiling by Wettability Modification on Nanometrically Smooth Surfaes", *Int. Comm. Heat Mass Transf*., 45, pp.11-15, (2013).

[8] McHale, J.P., Garimella, S.V., "Bubble Nucleation Characteristics in Pool Boiling of Wetting Liquid on Smooth and Rough Surfaces", *Int. J. Multiphase Flow*, 35, pp.249-260, (2010).

[9] Qi, Y., Klausner, F., Renwei, M., "Role of surface structure in heterogeneous nucleation", *Int. J. Heat Mass. Transf.*, 44, pp.4287-4311, (2001).

[10] Nimkar, D.N., Bhavnani, S.H., Jaeger, R.C., "Effect of Nucleation Sites Spacing on the Pool Boiling Characteristics of a Structured Surface", *Int. J. Heat Mass. Transf.*, 49, pp.2829-2839, (2006).

[11] Moita, A.S., Teodori, E., Moreira, A.L.N., "Enhancement of Pool Boiling Heat Transfer by Surface Micro-Structuring", *J. Physics: Conf. Series*, 935, pp.012175, (2012).

[12] Teodori, E., Moita, A.S:, Moreira, A.L.N., "Characterization of Pool Boiling Mechanisms over Micro-Patterned Surfaces Using PIV", *Int. J. Heat Mass Transf.*, 66, pp.261-270, (2013).

[13] Corty, C., Foust, A.S., "Surface Variables in Nucleate Boiling", *Chem. Eng. Prog. Symp.* Ser. 51(17), pp.1-12, (1955).

[14] Griffith, P. Wallis, G.B., "The role of Surface Conditions in Nucleate Boiling", *Chem. Eng. Prog. Symp.* Ser. 56, pp.49-63, (1960).

[15] Gartner, R.F., "Distribution of Active Sites in Nucleate Boiling of Liquids", *Chem. Eng. Prog. Symp.* Ser. 59, pp.52-61, (1963).

[16] Gartner, R.F., Westwater, J.W., "Population of Active Sites in Nucleate Boiling Heat Transfer", *Chem. Eng. Prog. Symp.* Ser. 56, pp.52-61, (1960).

[17] Sultan, M., Judd, J.L., "Spatial Distribution of Active Sites and Bubble Flux Density", *Trans. ASME J. Heat Transfer*, 100, pp.56-62, (1978).

[18] Del Valle. V.H.M., Kenning, D.B.R., "Subcooled Flow Boiling at High Heat Flux", *Int. J. Heat Mass Transfer*, 28, pp.1907-1920, (1985).

[19] Chu, K-H., Enright, R., Wang, E.N., "Structured Surfaces for Enhanced Pool Boiling Heat Transfer", *Appl. Phys. Lett.*, 100, pp.211603, (2012).

[20] Gerardi, C., Buongiorno, J., Hu, L-w., McKrell, T.,"Infrared Thermometry Study of Nanofluid Pool Boiling Phenomena", *Nanoscale Research Lett.*, 6, pp.232 (17pp), (2011).

[21] Gerardi, C., Buongiorno, J., Hu, L-w., McKrell, T., "Study of Bubble Growth in Water Pool Boiling Through Synchronized Infrared Thermometry and High-Speed Video", *Int. J. Heat Mass Transf.*, 53, pp.4185-4192, (2010).

[22] Han, C.Y., Griffith, P., "The Mechanism of Heat Transfer in Nucleate Boiling", Technical Report No 7673-19, M.I.T., (1962).

[23] Rohsenhow, W.M., "A Method for Correlating Heat Transfer Data for Surface Boiling of Fluids", *ASME J. Heat Transfer*, 74, pp.969-976, (1952).

[24] Jabardo, J.M.S., Silva, E. F., Barros, S. F. "Evaluation of the Rohsenow Correlation Throught Experimental Pool Boiling of Halocarbon Refrigerants on Cylindrical surfaces", *J. Braz. Soc. Mech. Sci. & Eng.*, Vol. XXVI, nº2, pp.218-230, (2004).

[25] Betz, A.R., Jenkins, J., Kim, C.-J., Attinger, D. "Boiling Heat Transfer on Superhydrophilic, Superhydrophobic and Superbiphilic Surfaces", *Int. J. Heat Mass Transf.*, 57, pp.733-741, (2013).

[26] Moita, A.S., Moreira, A.L.N., "Scaling the effects of surface topography in the secondary atomization resulting from droplet/wall interactions", *Exp. Fluids*, 52(3), pp.679-695, (2012).

[27] Abernethy, R.B., Benedict, R.P., Dowdell, R.B., "ASME Measurement Uncertainty", *J. Fluids Eng.*, 107(2), pp.161-164, (1985).

[28] Cheng, W., Murai, Y., Sasaki, T., Yamamoto M. "Bubble Velocity Measurement with a Recursive Cross Correlation PIV Technique", *Flow Meas. Instr*., 16, pp.35-46, (2005).

[29] Teodori, E., Moita, A.S., Moreira, A.L.N., "Pool Boiling Heat Transfer over Micro-Patterned Surfaces: Experiments and Theory", *8th World Conf. Exp Heat Transf., Fluid Mech. and Thermodynamics, ExHFT-8*, (2013).

[30] Fritz, W., "Maximum Volume of Vapor Bubbles", *Phys Z*, 36, pp.279-385, (1935).

[31] Gerardi, C., "Investigation of the Pool Boiling Heat Transfer Enhancement of Nano-Engineered Fluids by Means of High-Speed Infrared Thermography", PhD Thesis, M.I.T., (2009).